

# Chapter 5

## *Impact of Substrate and Furnace Atmosphere Composition on the Decomposition of a Commercial Cold Rolling Oil*

### **Preface**

This Chapter investigates the effect of two key process parameters on the thermal decomposition of a fully-formulated cold rolling oil; substrate (5.1) and furnace atmosphere (5.2) composition. In 5.1, iron is introduced into the rolling oil testing regime in the form of a cold rolled steel substrate and iron oxide powder, which is used to increase the iron-to-oil ratio and mimic the availability of iron fines formed by wear during cold rolling. The rolling oil thermo-oxidative decomposition process monitored by TGA under these two conditions is compared to that using an aluminium substrate. The impact of four different furnace atmospheres, from non-oxidising through to highly oxidising, on the oil decomposition process in the presence of a steel substrate is evaluated by TGA in 5.2. The activation energy associated with oil decomposition events is calculated in both sections by Modulated Thermogravimetry (MTGA) and the Flynn-Wall-Ozawa method. Furthermore, high temperature Laser Scanning Confocal Microscopy (LSCM) is used to visualise the process of rolling oil removal from the cold rolled steel surface (5.1). The results show that although the rolling oil thermo-oxidative decomposition process in the presence of the different substrates is similar, both steel and iron oxide powder act as oxidation catalysts and steel causes the formation of greater amounts of thermally-stable residue. LSCM shows that oil aggregation at sites of steel substrate oxidation could lead to high residue levels and represent a mechanism via which uncoated defects are formed. 5% hydrogen-95 % nitrogen is the optimal gas atmosphere for rolling oil decomposition as it promotes oil volatilisation at lower temperatures and minimises the formation of thermally-stable residues.

## 5.1 Effect of Substrate Composition on Rolling Oil Thermo-Oxidative Decomposition

### 5.1.1 Introduction

Iron is a well-known catalyst for the oxidation and cracking of hydrocarbons and is exploited within a range of industries to create useful products such as oils and fuels.<sup>1, 2</sup> Despite this utility, iron-catalysed oxidation has undesirable ramifications with respect to lubricant applications in the automotive and metal-working industries; oxidative degradation of lubricants at high temperatures results in the build up of sludge-like deposits that lead to wear and failure in mechanical systems<sup>3-11</sup> and cause coating problems in hot dip metal coated products.<sup>12-15</sup>

During the steel cold rolling process, a rolling oil film ( $\sim 300-600 \text{ mg m}^{-2}$ )<sup>16</sup> is applied to lubricate the steel surface. Iron is available for reaction with the rolling oil in two forms; the steel substrate and iron fines ( $\sim 20-100 \text{ mg m}^{-2}$ ),<sup>16</sup> small particles of steel produced by wear. Given that the rolling oil film must be cleanly removed from the steel surface prior to the continuous hot dip metallic coating process and that oil removal is typically achieved by ‘burn-off’ in a furnace containing natural gas combustion products, iron-catalysed oil oxidation reactions are of critical importance. However, the process of iron-catalysed rolling oil oxidation is poorly understood and the majority of research into rolling oil decomposition has been directed towards aluminium-catalysed oxidation of rolling oils used in cold rolling of aluminium<sup>17-19</sup> and oil decomposition under batch annealing (hydrogen or hydrogen/nitrogen mix) conditions.<sup>20-22</sup> The link between iron-catalysed oil oxidation and the formation of thermally-stable residues has primarily been investigated in relation to engine oils<sup>3, 4, 9, 23</sup> and minimal work has been done to study the analogous reactions in rolling oils.<sup>24</sup>

Thermogravimetric analysis (TGA) has long been used to evaluate the mechanism and kinetics of oil oxidation, decomposition and deposit formation. However, the majority of oils that have been analysed using this technique are once again used in the automotive industry.<sup>3, 4, 25</sup> The application of TGA to the analysis of cold rolling oils has been limited to studies of deposit formation, the effect of additives on oil residue and the

effect of cold rolled coil ‘aging’ on oil volatility.<sup>20, 26-28</sup> Similarly, high temperature LSCM is a useful technique for studying the temperature-dependent properties of materials and although it has been used extensively in the analysis of metallic phase transformations and microstructural development in steels,<sup>29, 30</sup> it has not been applied to visualise the process of rolling oil decomposition.

This work utilises TGA to compare the thermo-oxidative decomposition processes undergone by a fully-formulated commercial cold rolling oil in the presence of aluminium, low-carbon cold rolled steel and iron oxide powder. The activation energies of oil mass loss at different stages during the decomposition process have been evaluated by the Flynn-Wall-Ozawa<sup>31-33</sup> and MTGA techniques.<sup>34-36</sup> High temperature LSCM has been used to monitor the process of oil removal from the cold rolled steel surface and to visualise the formation and decomposition of oil-based deposits.

## **5.1.2 Experimental**

### **5.1.2.1 Sample Preparation**

#### **5.1.2.1.1 Materials**

This section of work focuses on the thermal decomposition characteristics of a fully-formulated oil, as opposed to additive/base ester blends. Formulation 560453 (refer to table 2.1 in Chapter 2 for composition and properties) was selected for analysis as it constitutes a suitable ‘reference’ oil via which to gauge the effect of different catalytic substrates; it contains none of the potentially problematic ingredients identified in previous Chapters (such as highly unsaturated base esters and sulfur EP additives) and industrial observations together with hot dip metallic coating simulation studies (refer to Chapter 6) have shown that it produces a high-quality coating free from uncoated defects.

Magnetite ( $\text{Fe}_3\text{O}_4$ , ‘iron oxide’) powder comprising of particles with an average diameter of 5  $\mu\text{m}$  was purchased from Sigma Aldrich and used as received. This powder was selected to replicate the iron fines formed by wear during the cold rolling process and to facilitate determination of the amount of iron exposed to oil in 50 % w/w rolling

oil/iron oxide powder blends (refer to section 5.3 for calculations).

The hexane, toluene, acetone and hydrochloric acid used clean steel pucks for use in TGA and LSCM experiments were purchased from Sigma-Aldrich Australia and were all of reagent grade.

The properties of the other materials used are described in Chapter 2 as follows:

- cold rolled steel - table 2.3;
- oxygen gas - section 2.2.6, and
- TGA consumables - section 2.2.7.

#### **5.1.2.1.2 Sample Preparation for TGA and MTGA**

To investigate the effect of different substrates in catalysing the rolling oil thermo-oxidative decomposition process, TGA and MTGA analyses were performed using the following sample configurations:

- rolling placed directly onto the surface of a platinum crucible (MTGA);
- rolling oil placed into an aluminium pan (TGA and MTGA);
- rolling oil paced onto the surface of a circular steel puck (TGA and MTGA), and
- 50 % w/w rolling oil/iron oxide powder mixture placed into an aluminium pan (TGA).

The 50 % w/w rolling oil/iron oxide powder blend was formulated by weighing the constituents into a glass vial and stirring manually until an homogeneous mixture was obtained (~ 5 mins). TGA analysis was undertaken immediately after mixture preparation to avoid oil oxidation due to storage. Several separate mixtures were analysed to ensure reproducibility.

6 mm and 8 mm diameter steel pucks were used to create oil/steel puck samples for TGA and MTGA experiments respectively. Figure 5.1 shows a schematic diagram of the oil/steel puck sample preparation procedure. The pucks were degreased in an ultrasonic bath in hexane, followed by acetone, followed by toluene (10 mins sonication in each solvent). They were then ‘pickled’ in a 10 % HCl solution at 75 °C for ~ 1 min, rinsed in de-ionised water and then in acetone and finally dried under a stream of nitrogen

immediately prior to analysis to create a consistent, fresh metal surface. An even film of rolling oil was placed onto the steel for TGA/MTGA analysis.

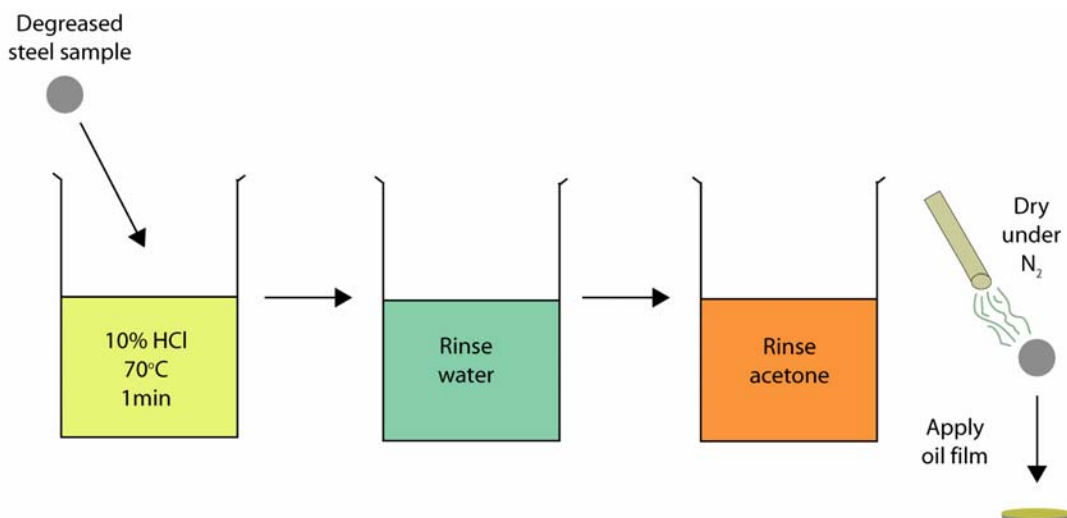


Figure 5.1 Schematic representation of rolling oil/steel sample preparation for TGA analysis.

The rolling oil/aluminium pan and rolling oil/platinum crucible samples were prepared by placing the desired mass of rolling oil directly onto the pan or crucible surface. Table 5.1 summarises the different TGA and MTGA sample configurations used.

Table 5.1 TGA and MTGA experiment summary.

Sample Configuration			Oil Mass (mg)	
Substrate	Container	Suspension from TGA Balance	TGA	MTGA
6 mm steel puck	-	Pt crucible	1	-
8 mm steel puck	-	Pt crucible	-	10
-	Al pan	Pt crucible	1	10
50 % w/w oil/iron oxide mixture	Al pan	Pt crucible	2	-
-	-	Pt crucible	-	10

### **5.1.2.1.3 Sample Preparation for High Temperature LSCM**

Sample preparation for high temperature LSCM was performed according to the procedure described in section 2.4.6 in Chapter 2.

## **5.1.2.2 Characterisation Techniques**

### **5.1.2.2.1 Conventional TGA**

TGA analysis using the various rolling oil/substrate configurations was carried out under oxygen according to the procedure described in Chapter 2.4.1 with the exception that 2 mg of 50 % w/w oil/iron oxide powder mixture, equivalent to 1 mg of rolling oil, was used (refer to table 5.1). Analyses were performed in triplicate at heating rates of 2, 5 and 10 °C min<sup>-1</sup>. Control runs were also performed using a steel puck with no rolling oil to assess the contribution of steel oxidation to the oil-steel curve. TA Instruments Specialty Library Software v1.00F was used to calculate kinetic parameters.

### **5.1.2.2.2 MTGA**

MTGA experiments were initially carried out using a range of different rolling oil masses, modulation periods and modulation amplitudes to optimise experimental conditions.<sup>37</sup> Ultimately, 10 ± 0.5 mg of rolling oil was selected as this was the minimum oil mass that could be used whilst providing an adequate mass % signal-to-noise ratio. The oil was spread onto the surface of an 8 mm diameter steel puck or placed into an aluminium pan or onto a platinum crucible for analysis (refer to table 5.1). A linear heating rate of 2 °C min<sup>-1</sup> was used together with a modulation period of 150 s and a modulation amplitude of ± 4 °C min<sup>-1</sup>. The instrumental temperature calibration was performed using the Curie temperatures of nickel and alumel standard reference materials (TA Instruments). Samples were equilibrated at 70 °C to reduce experimental running time and then heated using the above profile to 500 °C. Analyses were performed in duplicate and TA Instruments Universal Analysis 2000 v3.3B software was used to evaluate the data obtained.

### 5.1.2.2.3 High Temperature LSCM

High temperature LSCM analysis of rolling oil removal from cold-rolled steel was undertaken using the conditions and procedure outlined in section 2.4.6 in Chapter 2.

## 5.1.3 Results and Discussion

### 5.1.3.1 Conventional TGA

Conventional TGA analysis of the rolling oil was performed under oxygen in the presence of aluminium, steel and 50 % w/w iron oxide powder. Figure 5.2 shows an overlay of typical TGA results obtained. The DTG curve obtained using iron oxide powder has been scaled (multiplied by a factor of two) to enable effective comparison between the results. A summary of the onset points of mass loss ( $T_{\text{onset}}$ ), peak maximum temperatures ( $T_{\text{max}}$ ) and relevant mass losses and % residue levels at 500 °C is given in table 5.2.

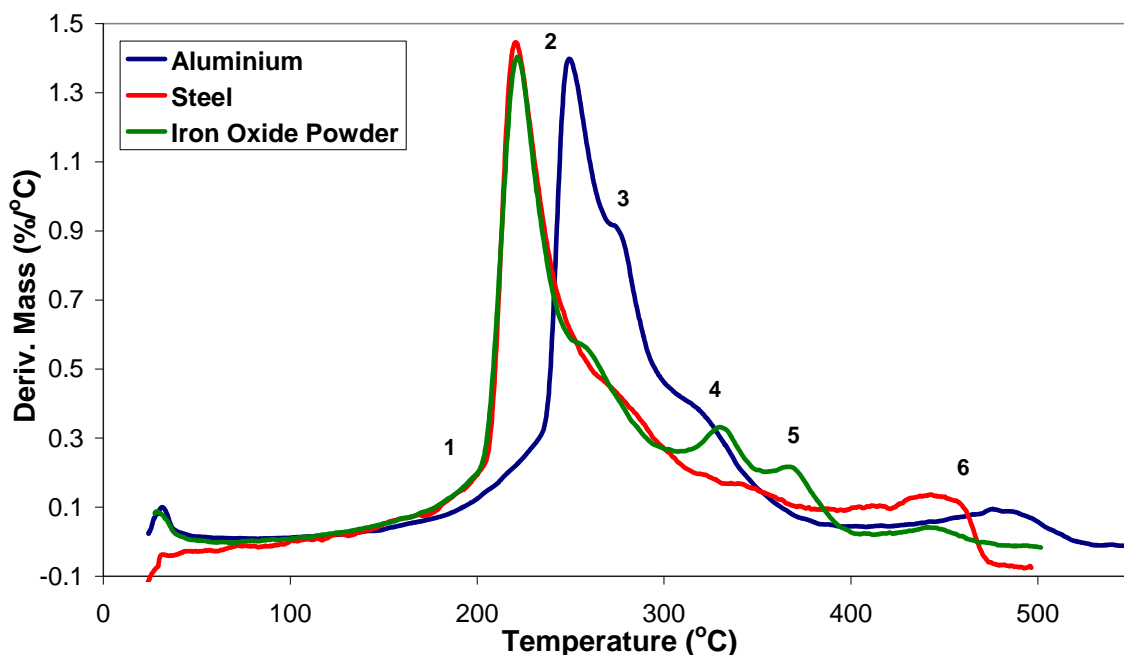


Figure 5.2 Overlay of the conventional TGA profiles (DTG curves) of the rolling oil thermo-oxidative decomposition process using steel, aluminium and 50 % w/w iron oxide powder catalysts. Events 1-6 are labelled on the curves.

**Table 5.2 Summary of TGA data for the rolling oil thermo-decomposition process in the presence of steel, aluminium and 50 % w/w iron oxide powder catalysts. Values given are the average of three individual runs and errors are less than  $\pm 15$  % for all measurements.**

Catalyst	$T_{\text{onset}}$ (°C)	Primary Region (Room Temperature-300 °C)						Secondary Region (> 300 °C)						% Residue at 500 °C	
		$T_{\text{max}}$ Event 1 (°C)	Mass Loss Event 1 (%)	$T_{\text{max}}$ Event 2 (°C)	Mass Loss Event 2 (%)	$T_{\text{max}}$ Event 3 (°C)	Mass Loss Event 3 (%)	$T_{\text{max}}$ Event 4 (°C)	Mass Loss Event 4 (%)	$T_{\text{max}}$ Event 5 (°C)	Mass Loss Event 5 (%)	$T_{\text{max}}$ Event 6 (°C)	Mass Loss Event 6 (%)		
		TGA	MTGA												
<i>Aluminium</i>	215	231	11.6	249	31.6	271	25.9	313*	21.5	-	-	477	7.38	2.7	1.2
<i>Steel</i>	191	210	7.25	226	43.0	274	32.1	-	-	-	-	434	10.3	6.6	2.5
<i>Iron Oxide Powder (50 % w/w)</i>	195	198	7.25	222	43.6	254	24.9	329	12.1	366	5.86	440	1.83	-	-

\* Event 3 in the steel results possibly contains a shoulder at  $\sim 320$  °C, however this shoulder is not evident in all three TGA runs.

The rolling oil thermo-oxidative decomposition profiles obtained using aluminium, steel and iron oxide powder mimic those observed for the commercial base esters studied in Chapter 3.2 (using aluminium substrate) and contain between four and six mass loss events. Given this similarity and that the rolling oil comprises ~ 65 % w/w esters, these events are likely to represent oil evaporation, oxidation, thermal cracking, reaction with the metal surface and the decomposition of thermally stable material (refer to discussion in Chapter 3.2).<sup>11, 20, 21, 23, 38</sup> The interdependency of the above reactions is highlighted by variations in the number of mass loss events observed between sample runs.

The rolling oil mass loss onset temperature is significantly lower in the presence of steel (191 °C) and iron oxide powder (195 °C) than aluminium (215 °C). Furthermore,  $T_{\max}$  for mass loss events 1 and 2 is more than 20 °C lower in the steel and iron oxide powder thermograms than in those obtained using aluminium ( $T_{\max}$  event 1 = 231 °C;  $T_{\max}$  event 2 = 249 °C). These observations are in agreement with the findings of Abou El Naga et al.,<sup>23</sup> who determined that iron is a better catalyst for oil oxidation than aluminium. The fact that the  $T_{\text{onset}}$  and  $T_{\max}$  values (other than the event 1  $T_{\max}$ ) measured for the rolling oil decomposition in the presence of aluminium are similar to the values determined for commercial base ester A in Chapter 3.2 confirms the dominance of the base ester thermo-oxidative decomposition process. However,  $T_{\max}$  for event 1 is ~ 56 °C higher in the commercial cold rolling oil formulation (the event 1  $T_{\max}$  measured for base ester A is 175 °C) due to the concurrent volatilisation of free fatty acids with low molecular weight oil additives such as emulsifiers ( $T_{\max}$  ~ 205 °C) and viscosity-boosting agents ( $T_{\max}$  ~ 235 °C; results obtained in a preliminary study of 17 rolling oil ingredients; refer to table 2.2 in Chapter 2).

Whilst the presence of iron has a significant impact upon  $T_{\text{onset}}$  and  $T_{\max}$  for events 1 and 2, increasing the oil to iron ratio (refer to section 5.3 below) from ~  $2.3 \times 10^{-7}$  moles of iron per 100 mg of rolling oil (steel) to ~  $1.6 \times 10^{-3}$  moles of iron per 100 mg of rolling oil (50 % w/w iron oxide powder) has comparatively little effect; the difference in  $T_{\text{onset}}$  is within experimental error and the  $T_{\max}$  values determined for events 1 and 2 are lowered by only ~ 10 °C. The small difference in the steel and iron oxide  $T_{\max}$  values

despite the significantly larger oil to iron ratio employed in the iron oxide powder tests results from the different catalytic activity of iron oxide as opposed to fresh metal surface. Furthermore, transition metals (such as manganese) present at the steel surface may be involved in catalysing oil oxidation reactions, accounting for the comparatively higher activity of the steel.<sup>23</sup>

The use of an iron-based catalyst also has a considerable effect on the proportion of oil mass lost over events 1 and 2; whilst 11.6 % of oil mass is lost during event 1 in the presence of aluminium, only 7.25 % is lost in the presence of steel and iron oxide powder. This results from overlap between events 1 and 2 in the steel and iron oxide powder results; in the presence of aluminium, events 1 and 2 are more discrete so that proportion of mass lost during event 1 is higher. In contrast, steel and iron oxide powder cause higher oil mass loss during event 2 (43.0 % and 43.6 % respectively) than aluminium (31.6 %). This can be rationalised by the accelerated rate of oil oxidation in the presence of steel and iron oxide powder in comparison to aluminium; the steel and iron oxide powder-catalysed samples form high concentrations of radicals (such as R<sup>•</sup>, RO<sup>•</sup> and ROO<sup>•</sup>) at lower temperatures. Although these conditions favour radical recombination, secondary decomposition reactions producing volatile species such as low molecular weight aldehydes, ketones, alcohols and acids are inevitable (refer to schemes 1.15-1.16 in Chapter 1), accounting for the greater levels of mass loss.<sup>39</sup>

Events 3, 4 and 5 occur in the temperature range 254–366 °C and give rise to a total of 32.1-47.4 % mass loss. As noted above, these events vary significantly between the aluminium, steel and iron oxide powder-catalysed samples and represent multiple processes including the further formation of radical recombination and secondary oxidation products, polymerisation, reaction with the substrate surface to form carboxylate, phosphate and/or sulfate species, decarboxylation and thermal cracking. The extent of this variation indicates that the equilibrium between reactions giving rise to volatilisation or the formation of thermally-stable residues is highly dependent upon catalyst composition. The aluminium-catalysed oil samples lose more mass over events 3 to 5 (47.4 %) than do the iron oxide powder-catalysed (38.0 %) and steel-catalysed

(32.1 %) samples due differences in the mechanism of oil decomposition. As noted above, the formation of higher concentrations of radicals in the presence of steel and iron oxide powder means that reactions leading to the evolution of non-volatile residues (such as radical recombination and polymerisation; refer to schemes 1.15 and 1.14 in Chapter 1 respectively) compete strongly with secondary oxidation reactions. These residue-forming reactions are less prevalent in the aluminium-catalysed oil samples as a result of the lower probability of radicals coming into contact with one another or with carbon-carbon double bonds,<sup>39</sup> enabling a greater proportion of oil mass to be lost during events 3-5.

Event 6, which represents the combustion of residual thermally-stable deposits such as carboxylates, high molecular weight radical recombination products, crosslinked material and inorganic components formed by phosphorus EP/AW additives and mineral oil-derived sulfur, occurs at significantly lower temperature in the presence of steel ( $T_{\max} = 434\text{ }^{\circ}\text{C}$ ) and iron oxide powder ( $T_{\max} = 440\text{ }^{\circ}\text{C}$ ) than aluminium ( $T_{\max} = 477\text{ }^{\circ}\text{C}$ ). This implies that iron is not only a better catalyst for rolling oil oxidation; it promotes the clean burn-off of persistent residues. Despite this, a similar proportion of mass is lost during event 6 for aluminium and steel (7.38 % and 10.3 % respectively) whereas the iron oxide powder samples lose significantly less ( $\sim 1.83\%$ ), suggesting that a lower proportion of thermally stable deposits are formed in the presence of iron oxide powder by the preceding oil decomposition reactions. Accordingly, the decomposition end temperature ( $T_{\text{end}}$ ) is shifted to increasingly lower value with the use of steel ( $T_{\text{end}} = 478\text{ }^{\circ}\text{C}$ ;  $T_{\text{end}}$  aluminium =  $524\text{ }^{\circ}\text{C}$ ) and iron oxide powder ( $T_{\text{end}} = 471\text{ }^{\circ}\text{C}$ ). The presence of iron fines in the industrial cold rolling process could therefore assist maintaining a steel surface that is free from oily residues. However, the residue level measured using steel (6.6 %) is higher than that measured using aluminium (2.7 %; the % residue cannot be measured for the 50 % w/w iron oxide powder samples as the starting mass of the powder cannot be accurately known). Although the steel substrate contribution to this residue measurement is  $\sim 2\%$  due to the commencement of substrate oxidation in the range  $470\text{-}480\text{ }^{\circ}\text{C}$ , subtraction of this mass increase from the % residue measured at  $500$

°C still infers that ~ 4.6 % oil-derived residue remains on the steel surface. Furthermore, the higher level of residue measured using steel is in agreement with the results reported by Sech et al.,<sup>20</sup> and suggests that a greater proportion of surface-bound material such as carboxylates, sulfates and phosphates is formed. When combined with the shift in  $T_{\text{end}}$  to lower temperature, this infers that the mass loss observed during event 6 represents the decomposition of organic as opposed metal salt-based material. This supports the findings made in Chapters 3 and 4 where ATR analysis showed that metal salts comprise a large proportion of the thermally stable deposits formed by the decomposition of ester and sulfur/phosphorus-based additives.

### 5.1.3.2 Activation Energy of Oil Decomposition

#### 5.1.3.2.1 Flynn-Wall-Ozawa Method

The kinetics of the rolling oil decomposition process using aluminium and steel substrates were analysed using the Flynn-Wall-Ozawa (non-isothermal)<sup>31-33</sup> and MTGA methods.<sup>34-36</sup> The method devised by Flynn and Wall and Ozawa enables the activation energy of a mass loss process to be determined from equation 5.1:

$$\log \beta = -0.457 \frac{E_a}{RT} + \left( \log \frac{AE_a}{RT} - \log F(\alpha) - 2.315 \right) \quad \text{Equation 5.1}$$

where  $\beta$  is the heating rate,  $T$  is the temperature,  $R$  is the gas constant,  $\alpha$  is the sample conversion,  $A$  is the pre-exponential factor and  $E_a$  is the activation energy. The slope of the straight line obtained by plotting  $\log \beta$  vs.  $1/T$  at any level of sample conversion can be used to calculate  $E_a$ .

Figure 5.3 shows a typical  $\log \beta$  vs.  $1/T$  plot for the oil decomposition process using an aluminium substrate. The straight lines are parallel between 20 and 40 % conversion, however at conversion levels above 40 % the line slope changes continuously and the fit to the data is not as good. The change in the line slope at 40 % conversion corresponds

to the event 2 peak temperature (249 °C) and indicates a change in the activation energy of oil decomposition.<sup>25, 40</sup>

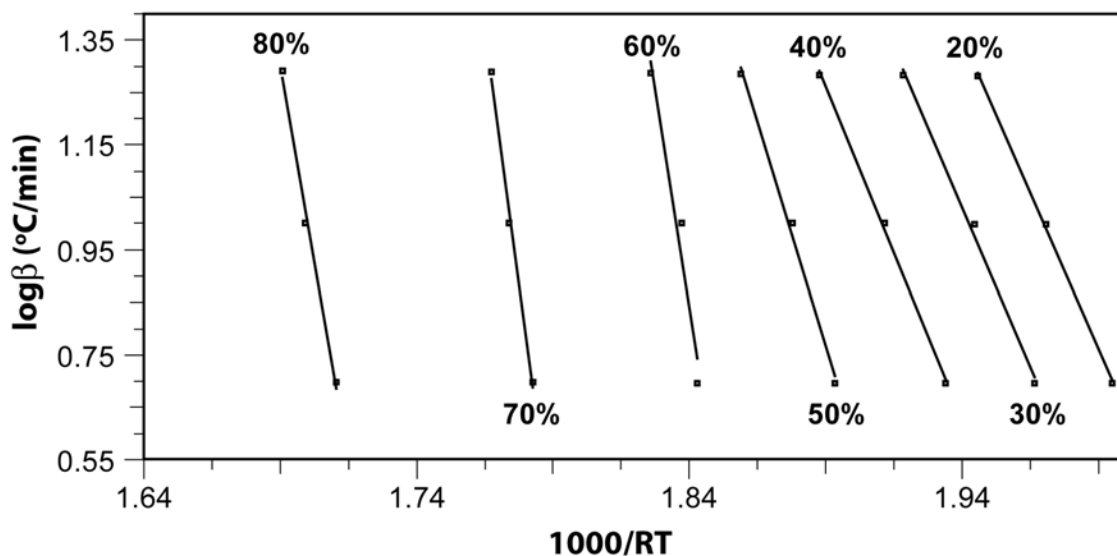


Figure 5.3 Logβ vs. 1/T plot for the rolling oil decomposition process using an aluminium substrate.

Subsequent changes in the line slope correspond to the commencement of event 3 (~ 50-75 % conversion) and event 4 (~ 80 % conversion) and evidence the complexity of the reactions giving rise to oil mass loss at higher conversion levels. The slope of the straight lines in logβ vs. 1/T plots obtained using a steel substrate also varies, confirming changes in the activation energy and mechanism of oil decomposition. However, the conversion level at which this variation is first observed is higher (~ 50 % conversion). In accordance with the mass loss mechanisms proposed for methyl esters and triglycerides/commercial base esters in Chapter 3, this implies that in the presence of a steel substrate, event 2 is dominated by thermo-oxidative decomposition reactions. Conversely, event 2 using an aluminium substrate involves a combination of oil evaporation (at lower conversion levels) and oxidative decomposition, giving rise to the observed change in mass loss mechanism at lower conversion levels. Table 5.3 summarises the activation energies ( $E_a$ ) of oil decomposition using aluminium and steel

substrates in the 20-90% conversion range.

**Table 5.3 Summary of activation energies obtained by the Flynn-Wall-Ozawa method between 20 and 90 % conversion using aluminium and steel substrates.**

Decomposition Event		Conversion Level (%)	Activation Energy, $E_a$ (kJ mol <sup>-1</sup> )	
			Aluminium	Steel
<i>Primary Region</i>	2	20	205	65
		30	173	66
		40	163	68
	3	50	205	72
		60	408	82
		70	465	90
<i>Secondary Region</i>	4	80	526	104
		85		84
	6	90		78

The results obtained using an aluminium substrate only enable  $E_a$  to be determined up to ~ 80 % conversion. At higher conversion levels the fit of the straight lines to the data is poor and  $E_a$  values cannot be validly determined. Despite this, the  $E_a$  values obtained at conversion levels below 80 % are in good agreement with those described by Santos et al.<sup>41</sup> for the thermo-oxidative decomposition of triglycerides using an aluminium substrate (~ 79-107 kJ mol<sup>-1</sup> and 205-349 kJ mol<sup>-1</sup> for the equivalents of events 2 and 3 respectively), verifying that the Flynn-Wall-Ozawa technique provides reliable kinetic information for the rolling oil thermo-oxidative decomposition process.

The initial  $E_a$  values measured in the presence of steel show that oil oxidation is already occurring at the 20 % conversion level;  $E_a$  commences at a low value (65 kJ mol<sup>-1</sup>) and subsequently increases. In contrast,  $E_a$  measured at 20 % conversion in the presence of aluminium is quite high (205 kJ mol<sup>-1</sup>) and coincides with the initial stages of

evaporation of high molecular weight oil constituents such as base esters. The aluminium 30-40 % conversion range witnesses a drop in  $E_a$  to a minimum of 163 kJ mol<sup>-1</sup>. This corresponds to the commencement of oil oxidation reactions, which are autocatalytic in nature.<sup>1, 17, 42</sup> The trend in both the aluminium and steel substrate data shows that  $E_a$  then gradually increases up to 526 kJ mol<sup>-1</sup> and 104 kJ mol<sup>-1</sup> respectively at 80 % conversion. The 50-80 % conversion region corresponds to event 3 and the initial stages of event 4, where numerous competing reactions (as outlined above) are occurring. The increases in  $E_a$  observed in the presence of both substrate types show that the residues formed by these reactions become increasingly more thermally stable and require more energy to volatilise as the oil decomposition process advances. At conversion levels above 80 %, the steel substrate data show that  $E_a$  decreases before stabilising at an average of 77 kJ mol<sup>-1</sup> as the oil decomposition process is completed. The  $E_a$  values measured using a steel substrate are consistently lower than those measured using aluminium, confirming the superior activity of steel in catalysing both the oil oxidation process and the decomposition of thermally stable deposits present at high temperatures.<sup>23</sup>

#### 5.1.3.2.2 MTGA

The rolling oil decomposition process was also studied by MTGA enabling  $E_a$  to be determined continuously as a function of conversion according to equation 5.2.<sup>34, 35, 37, 43, 44</sup>

$$E_a = \frac{R(T^2 - A^2)L}{2A} \quad \text{Equation 5.2}$$

where T is the average temperature, A is the temperature amplitude and L is the ratio of the natural logarithm of the maximum and minimum rate mass loss taken at adjacent half cycles of the sine wave. Figure 5.4 illustrates the MTGA results obtained using a platinum substrate, which was studied in addition to steel and aluminium substrates to

investigate the non-catalysed oil thermo-oxidative decomposition process.

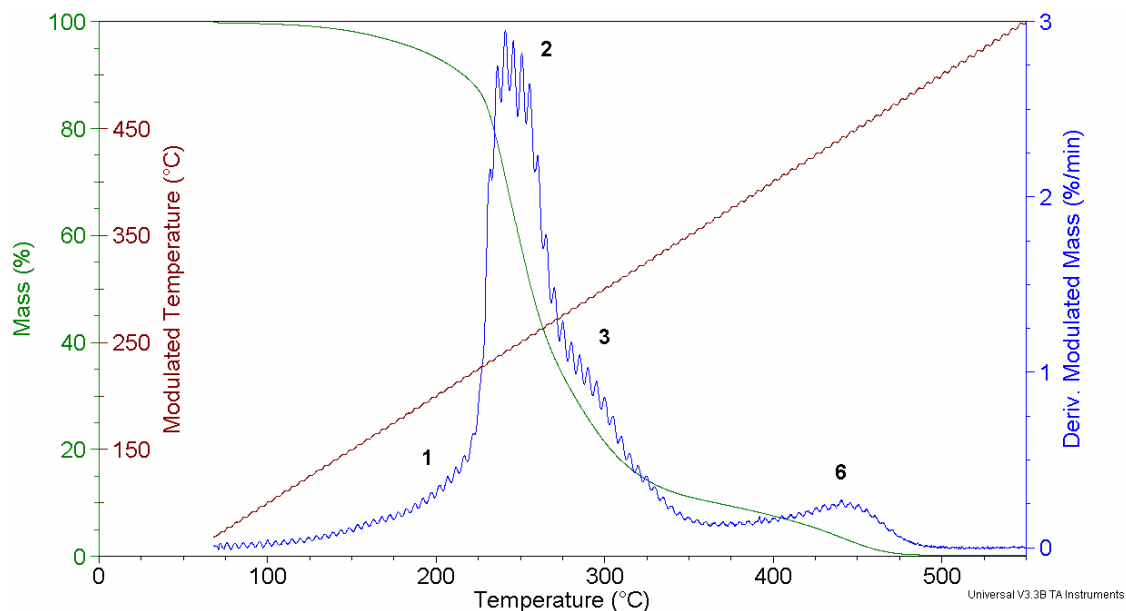


**Figure 5.4** MTGA results obtained using a platinum substrate. The modulated temperature, mass loss with respect to temperature (TG) and first derivative of modulated mass loss with respect to time (DTG) signals are shown. Mass loss events 1-6 are labelled on the DTG curve.

The oil decomposition process by MTGA is analogous to that observed by conventional TGA and proceeds via four mass loss events equivalent to events 1, 2, 3 and 6 in table 5.2. In accordance with the recommended conditions for use in MTGA experiments, more than five temperature modulation cycles occur within the temperature range over which each mass loss event occurs.<sup>35, 37</sup> This enables the activation energy of oil decomposition over each of these events to be accurately determined. Figure 5.5 shows a continuous  $E_a$  vs. conversion plot calculated for the oil thermo-oxidative decomposition process in the 10-95 % conversion range using a platinum substrate (5.5A) together with a comparison between  $E_a$  values measured using platinum, aluminium and steel substrates (5.5B). The Flynn-Wall-Ozawa results obtained using steel are included for comparative purposes.

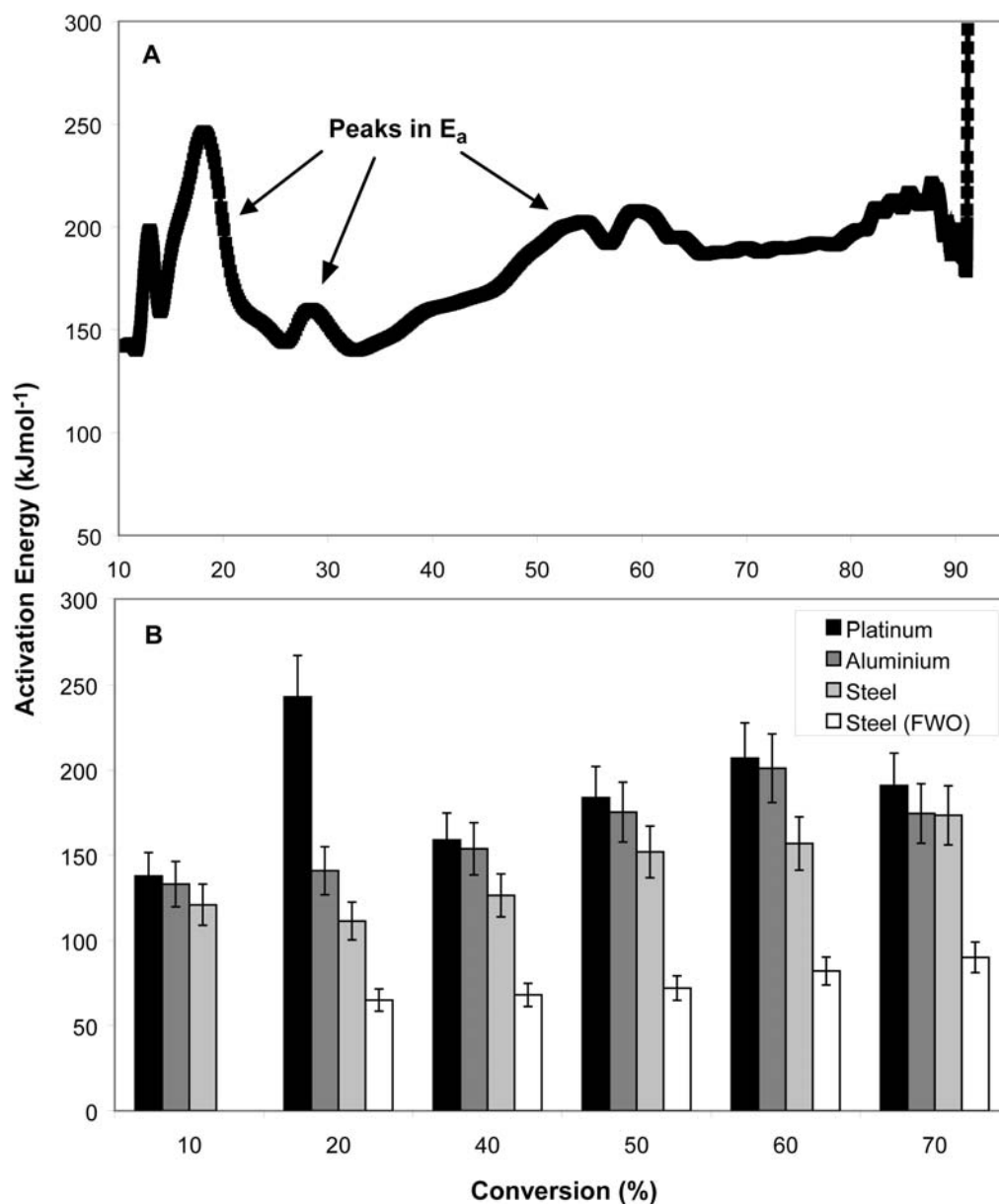


**Figure 5.5** Activation energy monitored continuously as a function of conversion for the oil decomposition process using a platinum substrate (A). Comparison between activation energies measured using platinum, aluminium and steel substrates at different conversion levels (B). Results obtained by the Flynn-Wall-Ozawa technique (FWO) are shown for comparison. The error bars represent  $\pm 10\%$  error.

The results presented in figure 5.5 verify that the steel substrate catalyses oil thermo-

oxidative decomposition by lowering the activation energy over the entire conversion range studied. A general increase in  $E_a$  with increasing sample conversion is observed for all three substrates, confirming that more energy is required to initiate the thermo-oxidative decomposition of oily residues present at higher temperatures. However, the  $E_a$  vs. conversion plots determined by MTGA differ from the Flynn-Wall-Ozawa results in that they display several peaks in  $E_a$  (shown for platinum in figure 5.5B), confirming that multiple reactions contribute to the oil thermo-oxidative decomposition process and highlighting the benefit of continuously monitoring changes in  $E_a$ .<sup>34, 35</sup> A summary of the conversion levels at which peaks in the activation energy of oil decomposition occur using the three different substrates is given in table 5.4.

**Table 5.4 Summary of conversion levels at which peaks occur in the activation energy of oil decomposition by MTGA.**

Decomposition Event		Conversion Level (%)	Peak in Activation Energy, $E_a$ (kJ mol <sup>-1</sup> )		
			Platinum	Aluminium	Steel
<i>Primary Region</i>	2	13	198		129
		18	246		
		23			119
		28	160		
	3	50		204	148
		55	203		149
		60	208		166
		65		191	197
		70		171	
		77			
<i>Secondary Region</i>	4	80-88	198-222		

The conversion levels at which peaks in  $E_a$  occur varies between the three substrates,

evidencing differences in the process of oil decomposition. The major  $E_a$  peaks observed for the oil decomposition from a platinum substrate correspond to the initial stages of event 2 (13 % and 18 % conversion), the event 2 maximum rate of mass loss temperature (28 % conversion), event 3 (55 % and 60 % conversion) and the latter stages of event 4 (series of peaks between 80 % and 88 % conversion). As noted by Gracia-Fernandez et al.,<sup>37</sup> these peaks in  $E_a$  correspond to the different mechanisms giving rise to oil mass loss. At 91 % conversion  $E_a$  tends towards infinity due to low levels of sample volatilisation.<sup>34, 37</sup> Consequently,  $E_a$  cannot be determined during the final mass loss event (event 6).

In contrast to these observations, the results obtained using aluminium and steel substrates show very few peaks in  $E_a$  at conversion levels below 45 %. This confirms that aluminium and steel catalyse the reactions giving rise to oil mass loss at low conversions. However at 50 and 65 % conversion, significant peaks in  $E_a$  are observed in the aluminium results, corresponding to the latter stages of event 2 and the commencement of event 3 respectively. The subsequent increase in  $E_a$  towards infinity occurs at a lower conversion level than for platinum at  $\sim 77$  %.<sup>34, 37</sup>

Similar features are observed in the steel results, however the conversion level at which  $E_a$  increases to infinity is lower at  $\sim 70$  %. This accounts for the greater level of residue at 500 °C detected using a steel substrate by both conventional (6.6 %) and modulated (2.5 %) TGA; the % residue at 500 °C measured using an aluminium substrate is 2.7 % and 1.2 % by TGA and MTGA respectively. The comparatively high conversion level at which  $E_a$  increases to infinity for the oil decomposition process using platinum evidences that oil volatilisation continues to proceed at higher temperatures and that lower levels of thermally stable oxidised and/or surface-bound deposits are formed.

Comparison between the MTGA and Flynn-Wall-Ozawa results obtained using a steel substrate (figure 5.5B) shows that the activation energy values determined by MTGA are at least 45 kJ mol<sup>-1</sup> higher than those measured by the Flynn-Wall-Ozawa technique. In accordance with the autocatalytic nature of oil oxidation<sup>1, 17, 42</sup> and with findings made for the analysis of engine oils,<sup>35</sup> this suggests that the oil thermo-oxidative

decomposition process generates significant amounts of heat. This results in a greater contribution to the heating part of the sinusoidal temperature cycle so that a higher average temperature value is measured according to equation 5.2. Consequently, the  $E_a$  values calculated from MTGA data are greater than those determined using the Flynn-Wall-Ozawa procedure.

The  $E_a$  values determined by the MTGA and Flynn-Wall-Ozawa techniques using an aluminium substrate are closer in value, suggesting that a lesser amount of heat is evolved during the oil oxidation process. This is once again consistent with the inferior catalytic activity of aluminium. A comparison between the activation energies determined by the Flynn-Wall-Ozawa and MTGA techniques therefore provides significant information on the nature of mass loss processes.

### **5.1.3.3 High Temperature LSCM**

Visualisation of the rolling oil decomposition process using a steel substrate was achieved using high temperature LSCM. Figure 5.6 shows images acquired at different stages during the oil decomposition process.

The first image, acquired at  $\sim 144$  °C, corresponds to the initial stages of oil mass loss by TGA. The majority of the steel substrate is covered by the oil film, however the appearance of an area of exposed steel substrate in the bottom right hand corner of the image confirms the commencement of oil evaporation. The black spots visible on the steel substrate are sites of oxidation; analogous features are apparent in images acquired of a steel control sample.

The image at 184 °C visualises the oil volatilisation process close to the TGA onset point of mass loss (191 °C). A vast proportion of the oily film has been removed from the steel surface, however ‘islands’ of oil appear as bright patches surrounding numerous sites of oxidation. Accumulation of the rolling oil at these sites represents a potential mechanism via which uncoated defects are formed; the concentration of oil residues at specific locations on the steel surface could lead to increased levels of thermally-stable deposits.

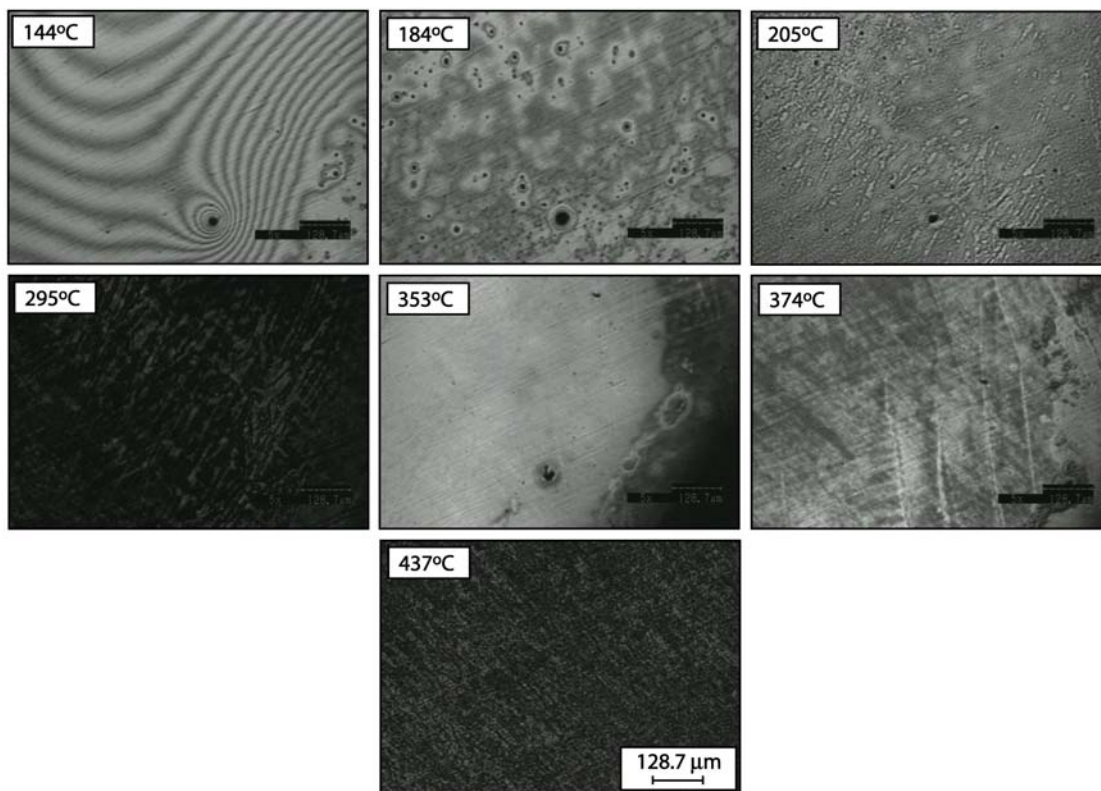
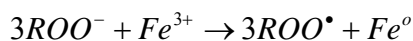


**Figure 5.6** High temperature laser scanning confocal microscopy images captured at a series of different temperatures during the rolling oil thermo-oxidative decomposition process.

At 205 °C the bright patches of oil have diminished in size and reflectivity, confirming that a significant proportion of oil mass has been converted to volatile products. This temperature corresponds to the maximum rate of mass loss temperature by TGA (210 °C) and marks a change in the mechanism of oil mass loss. Several sites of substrate oxidation (dark spots) are still apparent. At the end of the TGA primary decomposition region (~ 295 °C) significant changes in the sample appearance are evident. The surface is much darker as a result of reduced reflectivity, corresponding to the formation of oxidised oil residues. These residues are removed from the surface by 353 °C, as indicated by the increased reflectivity (light colour) of the steel surface. This temperature corresponds to the regime during which radical recombination, thermal cracking and metal carboxylate formation reactions are occurring. A reduction in the

number of black spots on the surface implies that oxides are reduced back to metal by reaction with hydrocarbons. This is in agreement with the reactions proposed by Abou El Naga et al.<sup>23</sup> whereby carboxylates can be oxidised by iron oxides to form oxygenated radical species according to scheme 5.1.



**Scheme 5.1 Redox reaction between carboxylate anions and iron(III) oxide to form peroxide radicals and metallic iron.**

At 374 °C (between TGA mass loss events) the steel substrate is beginning to darken due to oxidation. This confirms that the majority of oil deposits have been volatilised (evidence of oily deposits is evident in the bottom right hand corner of the image, which remains quite reflective). No further oil decomposition processes are evident at higher temperatures (up to 600 °C) as evidenced by consistent surface reflectivity. This confirms that the surface darkening first observed at 374 °C, and more obvious at 437 °C, is due to substrate oxidation.

#### **5.1.4 Conclusions**

The similarity in the rolling oil thermo-oxidative decomposition behaviour observed using aluminium, steel and 50 % w/w iron oxide powder catalysts confirms that an aluminium substrate can be validly used to mimic rolling oil removal from cold rolled steel. Despite this, the presence of iron in the catalytic material shifts the oil volatilisation processes to lower temperature, an effect which is compounded by increasing the iron to oil ratio. The level of oily residue remaining at 500 °C is increased by the use of a steel substrate, an observation which can be attributed to oil reactions with the substrate surface to form metal salts.

The activation energies measured the Flynn-Wall-Ozawa and MTGA methods confirm the superior activity of steel in catalysing oil oxidation. However, the increase in

activation energy observed with increasing conversion using both steel and aluminium substrates evidences that the residues formed become more thermally stable as the oil decomposition process advances. MTGA provides a unique insight into the mechanisms giving rise to oil volatilisation and variation between the activation energies determined by MTGA and the Flynn-Wall-Ozawa method is indicative of the exothermic or endothermic nature of oil decomposition reactions.

The images obtained by LSCM confirm the identity of oil thermo-oxidative decomposition reactions but also suggest that substrate oxidation may play a significant role in the residue formation process; the formation of isolated areas of surface oxides could nucleate the aggregation of oily residues and potentially account for the observance of uncoated defects in hot dip metallic coatings. Evidence of redox chemistry between the steel substrate and carboxylate-based residues was also detected.

## **5.2 Effect of Furnace Atmosphere Composition on Rolling Oil Removal from Cold Rolled Steel**

### **5.2.1 Introduction**

Oil-based lubricants are commonly used in metal-forming processes. One such process is the cold rolling of sheet steel where a lubricating oil, a complex formulation of more than ten different ingredients, must be capable of satisfying several different, and often competing, requirements.<sup>45, 46</sup> One of these requirements is that the oil must be easily removed from the steel surface prior to the application of hot-dip metallic coatings. Common oil removal methods include alkaline, acid or electrolytic degreasing,<sup>15</sup> however many metal coating lines elect to remove the rolling oil via treatment in a furnace. Furnace treatment enables simultaneous cleaning of the steel strip surface and modification of the physical properties of the steel. Two of the most common furnace set-ups used are ‘batch annealing’ and ‘continuous annealing’. In the batch annealing process, cold rolled coils stacked within a furnace containing a mixture of hydrogen and nitrogen gases are heated at slow ( $1.7\text{ }^{\circ}\text{C min}^{-1}$ ) heating rates to approximately  $690\text{ }^{\circ}\text{C}$ .<sup>21</sup>

Continuous annealing incorporates a dual furnace system. Removal of residual oil on the steel surface occurs within a furnace containing natural gas combustion products and nitrogen. The heating rates within this furnace are estimated to be approximately  $6500\text{ }^{\circ}\text{C min}^{-1}$  and the final steel temperature is approximately  $500\text{ }^{\circ}\text{C}$ . The steel then passes through a furnace containing a low dew point, hydrogen-nitrogen atmosphere under which steel surface oxides are reduced.<sup>47</sup>

Effective removal of the rolling oil from the steel surface in both batch and continuous annealing is critical to the quality of subsequent surface treatments and coatings; the formation of thermally stable oil residues is highly detrimental to downstream processing.<sup>12-16, 20, 45, 48</sup> Several different chemical processes have been identified as contributing to overall oil removal including evaporation, oxidation and decomposition resulting in the formation of volatile products.<sup>3, 4, 17, 49</sup> The precise balance between each of these processes and the extent to which the equilibrium between them can be manipulated to optimise steel surface cleanliness in the metallic coatings industry is largely unknown. In addition, whilst much work has been undertaken to identify the different reactions that occur in the rolling oil removal process under batch annealing conditions,<sup>20-22</sup> little has been done to investigate the reactions that occur under oxidising conditions. An improved understanding of the oil removal process and how the atmosphere in which oil removal occurs influences this process is of considerable interest and will aid in product development within the steel and lubricant industries.

In this study TGA has been employed to investigate how cold rolling oil is removed from the surface of low-carbon steel. A range of industrial furnace conditions, from non-oxidising through to highly oxidising, have been simulated by performing the TGA tests under argon, 5 % hydrogen-95 % nitrogen gas mixture, nitrogen and oxygen. The activation energies of oil removal,  $E_a$ , under each of these gas atmospheres have been determined by both MTGA<sup>34-36, 43</sup> and the Flynn-Wall-Ozawa<sup>31-33</sup> method to establish an optimal furnace atmosphere for rolling oil removal.

## **5.2.2 Experimental**

## **5.2.2.1 Sample Preparation**

### **5.2.2.1.1 Materials**

Rolling oil formulation 560453 (refer to table 2.1 in Chapter 2) was selected for analysis in this section for the reasons outlined in section 5.1.2.1.1 above. The hexane, toluene, acetone and hydrochloric acid used to clean steel pucks for use in TGA experiments are also described in section 5.1.2.1.1. The properties of the other materials used are described in Chapter 2.2 as follows:

- cold rolled steel - table 2.3;
- oxygen, nitrogen, HNX and argon gases - section 2.2.6, and
- TGA consumables - section 2.2.7.

### **5.2.2.1.2 Sample Preparation for TGA and MTGA**

All rolling oil samples analysed in this section were prepared on 6 mm diameter (TGA) or 8 mm diameter (MTGA) steel pucks according to section 5.1.2.1.2 above.

## **5.2.2.2 Characterisation Techniques**

### **5.2.2.2.1 Conventional TGA**

TGA analysis of rolling oil/steel samples was carried out under oxygen, argon, nitrogen and HNX gases according to the conditions and procedure described in section 2.4.1 in Chapter 2. Analyses were performed at heating rates of 2, 5 and 10 °C min<sup>-1</sup> and control runs using a steel puck with no rolling oil were undertaken to assess the contribution of steel oxidation to the oil-steel curve. All TGA experiments were performed in triplicate. TA Instruments Specialty Library Software v1.00F was used to calculate kinetic parameters.

### **5.2.2.2.2 MTGA**

MTGA analysis of rolling oil/steel samples was performed under oxygen, argon, nitrogen and HNX gases according to section 5.1.2.2.2 above.

## 5.2.3 Results and Discussion

### 5.2.3.1 Conventional TGA

The rolling oil decomposition process was studied by conventional TGA under each of the four gas atmospheres (argon, HNX, nitrogen and oxygen). Figure 5.7 presents the results obtained under nitrogen.

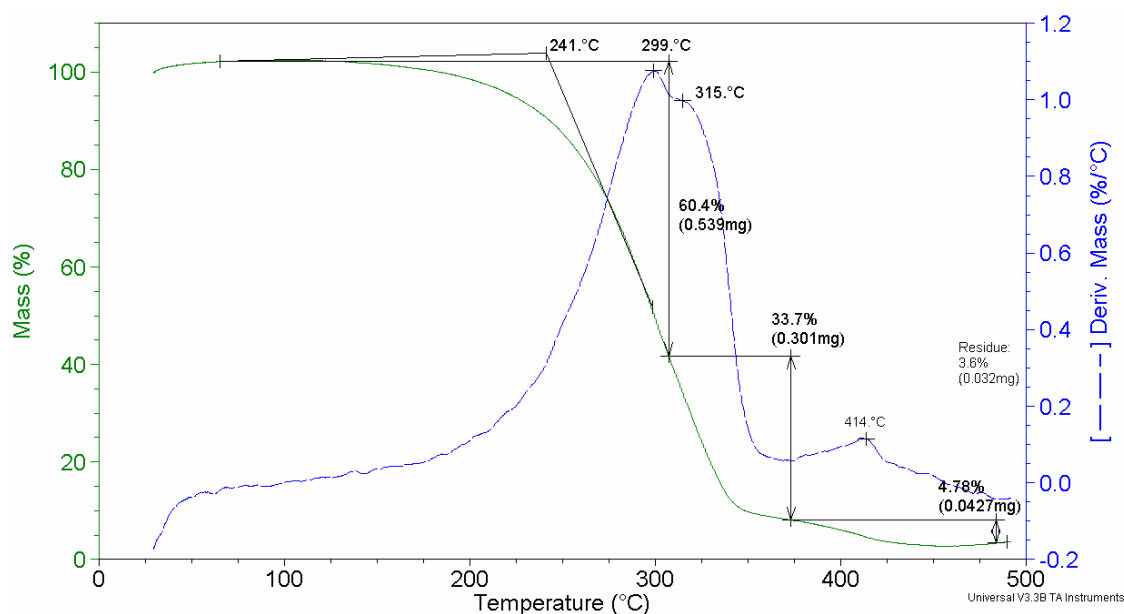


**Figure 5.7 Conventional TGA results obtained for the rolling oil decomposition under nitrogen. Both the mass loss with respect to temperature (TG) and first derivative of mass loss with respect to temperature (DTG) curves are presented.**

The oil decomposition process is analogous to that reported in the literature<sup>11, 20</sup> and comprises of three mass loss events. In accordance with the findings presented in 5.1 and Chapter 3, these events are likely to be dominated by ester evaporation, thermal cracking/reaction with the steel surface and the decomposition of thermally stable material respectively.<sup>11, 20, 21, 23, 38</sup> Event 1 occurs at a peak maximum temperature of ~ 294 °C and the majority of the oil mass (57.8 %) is converted to volatile products over this event. Although event 2 is largely superimposed upon event 1, it can be

distinguished by a separate peak in the DTG curve at 310 °C and corresponds to a further 34.9 % mass loss. The final mass loss event (event 3) occurs at 410 °C and gives rise to only 4.2 % mass loss such that 5.2 % residue remains at 500 °C. As noted in 5.1, the composition of this residue is likely to be carboxylate-, phosphate- and/or sulfate-based.<sup>24</sup> The results obtained under the other atmospheres follow this trend and a summary of the onset points of mass loss ( $T_{\text{onset}}$ ), peak maximum temperatures ( $T_{\text{max}}$ ) and corresponding mass losses and % residue at 500 °C is given in table 5.5.

The oil decomposition process under oxygen is described in detail in 5.1. It should be noted that event 1 is unique to the rolling oil decomposition in the presence of oxygen as it represents oil evaporation prior to the commencement of oxidation reactions. Given that oil oxidation is minimal under the other gas environments, a single evaporative mass loss event (event 2) is observed under argon, HNX and nitrogen. In order to compare levels of oil volatilisation between oxygen and the other gas atmospheres, the total mass loss occurring under oxygen during events 1 and 2 (50.9 %) will be referred to as event 2 mass loss. In accordance with the findings made in Chapter 3 and with the literature,<sup>1, 50</sup> the  $T_{\text{onset}}$  and event 2 and 3  $T_{\text{max}}$  values are lower under oxygen than under any of the other gases, evidencing the diminished thermal stability of the oil under oxidising conditions. The proportion of oil mass lost over events 2 and 3 is also lower under oxygen, indicating that whilst the oil decomposition process commences at lower temperature, less volatile matter is evolved in comparison to the other gas environments. This is due to the formation of non-volatile oxidation products as discussed in detail in Chapter 3 and outlined by schemes 1.14-1.15 in Chapter 1.<sup>1, 5, 39, 51-53</sup>

The event 4 peak temperature and mass loss under oxygen are much higher than those recorded under the other gases, confirming that more residual matter is left on the steel surface under oxygen after the initial oil removal process and that this residue is considerably more thermally stable. Despite the large proportion of event 4 oil mass lost under oxygen, the second largest amount of oil residue remains on the steel surface at 500 °C (6.6 %). Only under argon is the amount of residue higher (14 %). This results from the evolution of less volatile matter due to the non-reactivity of argon with the oil.

**Table 5.5 Summary of TGA data obtained for the rolling oil decomposition under each of the gas atmospheres investigated. Values given are the average of three individual runs and errors are less than  $\pm 15\%$  for all measurements except the % residue at 500 °C and the mass loss over event 3 ( $\pm 20\%$ ).**

Gas	$T_{\text{onset}} (^{\circ}\text{C})$	Primary Region (Room Temperature-300 °C)				Secondary Region (> 300 °C)				% Residue at 500 °C
		$T_{\text{max}}$ Event 1 (°C)	Mass Loss Event 1 (%)	$T_{\text{max}}$ Event 2 (°C)	Mass Loss Event 2 (%)	$T_{\text{max}}$ Event 3 (°C)	Mass Loss Event 3 (%)	$T_{\text{max}}$ Event 4# (°C)	Mass Loss Event 4# (%)	
<i>Argon</i>	218	-	-	273	51.3	302	36.5	417	3.91	14
<i>Nitrogen</i>	233	-	-	294	57.8	310	34.9	413	4.28	5.2
<i>HNX</i>	220	-	-	284	56.5	300	32.5	405	5.71	5.0
<i>Oxygen</i>	191	210	7.25*	226	43.6*	274	32.1	434	10.3	6.6

\* The total mass loss occurring during events 1 and 2 under oxygen is 50.9 %.

# Note that event 4 is equivalent to event 6 in 5.1.

The lowest event 4 peak temperature (405 °C) for the rolling oil decomposition process is measured under the reducing HNX atmosphere. This observation suggests that the residual oil present on the steel substrate following events 2 and 3 is less thermally stable under reducing conditions than under oxidising conditions. Decomposition of the oil under HNX also produces the least amount of residue at 500 °C (5.0 %). As described for the commercial base esters studied in Chapter 3.2, this lower level of residue can be attributed to the formation of unique volatile products (such as CH<sub>4</sub>) under HNX by oil reaction with gaseous hydrogen (refer to scheme 1.20 in Chapter 1).<sup>21, 54</sup> This is supported by the findings of Dionne et al.<sup>55</sup> who noted that increasing the hydrogen content of an HNX annealing atmosphere promotes the removal of carbon on the steel surface. Although volatiles (such as CO and CO<sub>2</sub> via the decarboxylation, combustion and high temperature reactions outlined by schemes 1.17, 1.19 and 1.20 in Chapter 1)<sup>21, 22</sup> are also produced under oxidising conditions, the additional reaction pathway available under HNX promotes oil volatilisation and minimises the formation of thermally stable residues. Achieving a lower event 3 peak temperature and a lesser amount of residue following oil decomposition would be highly beneficial in the industrial process.<sup>20, 55</sup>

The highest T<sub>onset</sub> (233 °C) and event 2 T<sub>max</sub> (294 °C) together with the greatest amount of event 2 mass loss (57.8 %) are observed under nitrogen. This is of considerable interest as it shows that a neutral (neither oxidising nor reducing) environment promotes volatilisation of the rolling oil at low temperatures and suggests that increasing the number of furnace zones fired under nitrogen could aid in achieving improved surface cleanliness in the continuous annealing process. Similar results are obtained under argon, although the onset point (218 °C) and event 2 peak temperature (273 °C) values are shifted to lower temperature. This is most likely to be due to the higher thermal conductivity of argon. The lesser amount of oil mass loss over events 2 and 4 under argon could result from a variation in the kinetics of the oil volatilisation reactions together with the non-availability of gaseous reactants such as O<sub>2</sub> and H<sub>2</sub>. Heating the oil more rapidly in the absence of these gaseous reactants favours deposit formation via the

hydrocarbon cracking reactions outlined in scheme 1.18 in Chapter 1.<sup>21</sup>

### 5.2.3.2 Activation Energy of Oil Decomposition

#### 5.2.3.2.1 Flynn-Wall-Ozawa Method

Kinetic analysis of the rolling oil decomposition process under each of the four gas atmospheres using the Flynn-Wall-Ozawa (non-isothermal) technique<sup>31-33</sup> yields  $\log\beta$  vs.  $1/T$  plots similar to that shown in section 5.1. Variations in the slope of the straight lines plotted at different conversion levels correspond to changes in the activation energy and mechanism of oil decomposition such that event 2 covers 0-50 % conversion, event 3 covers 50-75 % and event 4 occurs at conversion levels  $\geq 75$  %.<sup>25, 40</sup> A summary of the activation energies ( $E_a$ ) between 20 and 90 % conversion is given in table 5.6.

**Table 5.6 Summary of activation energies between 20-90 % conversion under each gas atmosphere.**

Decomposition Event	Conversion Level (%)	Activation Energy, $E_a$ (kJ mol <sup>-1</sup> )			
		Argon	Nitrogen	HNX	Oxygen
2	20	100	78	140	65
	30	102	79	145	66
	40	104	77	148	68
3	50	119	74	153	72
	60	131	72	157	82
	70	142	71	160	90
4	80	154	71	164	104
	82	154	71	161	96
	84	154	71	157	89
	86	152	71	155	79
	88	149	70	155	75
	90	146	69	159	78

The  $E_a$  values measured under HNX are at least  $40 \text{ kJ mol}^{-1}$  higher than those measured under the other gas atmospheres. This is due to the reactive as opposed to evaporative character of the processes giving rise to oil mass loss.  $E_a$  determined under oxygen is not similarly high as a result of the autocatalytic nature of oil oxidation reactions.<sup>1, 17, 42</sup> The lowest  $E_a$  values are measured under nitrogen ( $69\text{-}79 \text{ kJ mol}^{-1}$ ) and are in good agreement with those reported for the catalysed decomposition of rubber seed oil.<sup>56</sup>

At conversion levels below  $\sim 80 \%$ ,  $E_a$  increases as the oil decomposition process proceeds under every gas atmosphere except for nitrogen. This shows that the residues left on the steel surface become more thermally stable as the oil decomposition process advances. The fact that  $E_a$  under nitrogen at low conversion is greater than at higher conversion enables a large proportion of oil mass to be converted to volatile products over event 2.

Under oxygen, HNX and argon, the maximum  $E_a$  occurs at a conversion of  $80 \%$ . This conversion level corresponds to the commencement of event 4 where a greater amount of energy is required to initiate the removal of thermally stable oil residue. At conversion levels above  $80 \%$  the activation energy under each of the gases gradually decreases as the oil decomposition reactions represented by event 4 conclude.

#### 5.2.3.2.2 MTGA

Analysis of the rolling oil thermal decomposition process by MTGA yields the results presented in figure 5.8 (obtained under an atmosphere of argon). The oil decomposition process proceeds via three mass loss events and, as noted in section 5.1, is consistent with the decomposition profile observed by conventional TGA.

Figure 5.9 shows a typical plot of  $E_a$ , determined by both the MTGA and Flynn-Wall-Ozawa methods, as a function of conversion under argon. Similar plots were obtained under the other gas atmospheres. In contrast to the Flynn-Wall-Ozawa results, the  $E_a$  vs. conversion curve by MTGA displays several peaks confirming that multiple reactions contribute to the oil decomposition process and highlighting the benefit of continuously monitoring changes in  $E_a$ .<sup>34, 35</sup> The conversion levels at which these peaks occur

correspond to the transitional regions between different mass loss events (refer to table 5.6). In accordance with the proposed mechanisms of mass loss represented by event 3 (thermal cracking and reaction with the steel surface), two peaks are observed at ~ 45 % and 55 % conversion.

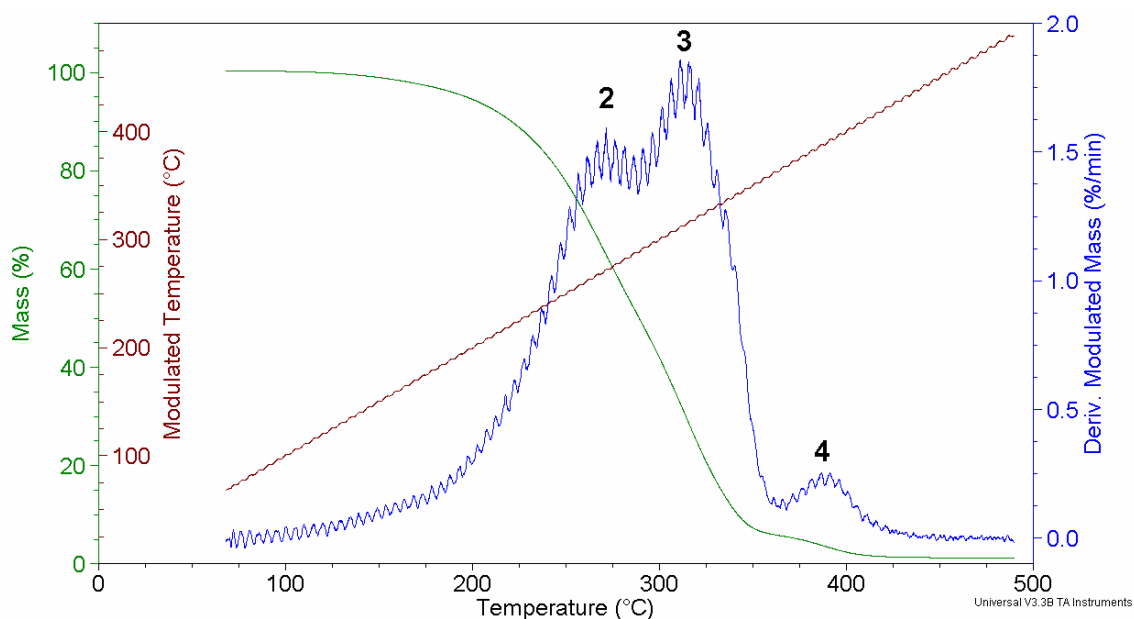


**Figure 5.8** MTGA results obtained under argon. The modulated temperature, mass loss with respect to temperature (TG) and first derivative of modulated mass loss with respect to time (DTG) signals are shown. Mass loss events 2-4 labelled on the DTG curve.

The MTGA data support the findings made by Flynn-Wall-Ozawa analysis; an increase in  $E_a$  is observed with increasing sample conversion under all gases except nitrogen, confirming that more energy is required to initiate the removal of oily residues present at higher temperatures. The activation energy for oil removal determined by Flynn-Wall-Ozawa analysis is at least  $35 \text{ kJ mol}^{-1}$  lower than that measured by MTGA under every gas atmosphere except HNX. This is consistent with the findings presented in 5.1 and suggests that the rolling oil decomposition process under gases other than HNX evolves significant amounts of heat.<sup>35</sup>

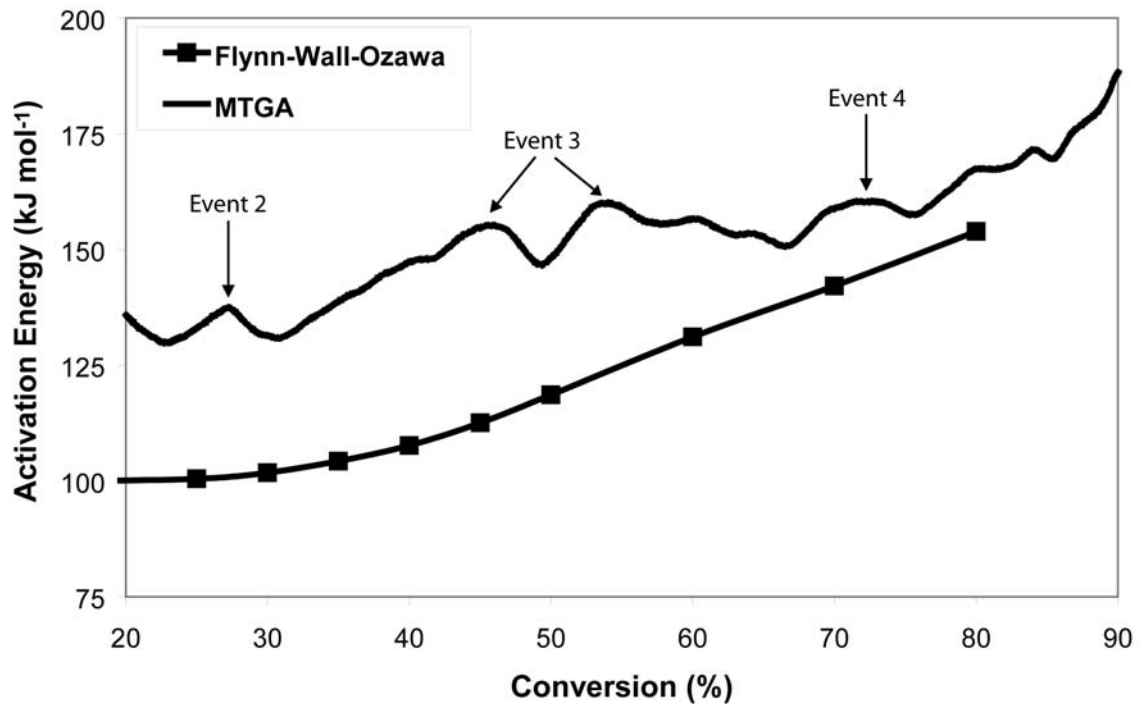


Figure 5.9 Activation energies calculated as a function of conversion from MTGA and Flynn-Wall-Ozawa results under argon.

#### 5.2.4 Conclusions

TGA has been used to study the process via which commercial cold rolling oil is removed from low-carbon steel under a range of gas atmospheres. The results show that a reducing atmosphere of 5 % hydrogen-95 % nitrogen is the optimal gas environment for effective removal of rolling oil from steel as a greater amount of oil mass is lost at lower temperatures and less thermally stable products are formed. This increased oil removal efficiency corresponds to higher activation energy as measured by the MTGA and Flynn-Wall-Ozawa techniques. A highly oxidising atmosphere has detrimental effects on the oil removal process as it causes the formation of thermally stable products and high amounts of residue within the maximum temperature range employed in the industrial furnace cleaning process.

## 5.3 Iron:Oil Ratio Calculations

### 5.3.1 Introduction

This section is aimed at estimating the iron to oil ratio present in the following:

- a 50 % w/w mixture of iron oxide powder and rolling oil;
- 1 mg of rolling oil on the surface of a 6 mm diameter steel puck, and
- the industrial cold rolling process (~ 600 mg rolling oil per m<sup>2</sup> of steel).

### 5.3.2 Calculations

#### 5.3.2.1 50 % w/w Oil/Iron Oxide Powder Mixture

The 50 % w/w oil/iron oxide powder mixtures used in section 5.1 were prepared using ~ 100 mg of magnetite (Fe<sub>3</sub>O<sub>4</sub>) powder and ~ 100 mg of rolling oil. The Fe<sub>3</sub>O<sub>4</sub> powder comprises of particles that are approximately 5 μm in diameter.

Assumptions:

- exactly 100 mg of powder and 100 mg of rolling oil are used in the mixtures;
- all particles in the powder are 5 μm in diameter;
- the particles are spherical and have a smooth surface, and
- the powder is 100 % Fe<sub>3</sub>O<sub>4</sub>.

##### 5.3.2.1.1 Total Number of Moles of Fe (II, III)

Mass of Fe<sub>3</sub>O<sub>4</sub>,  $m_{\text{Fe}_3\text{O}_4} = 100 \text{ mg}$ .

Molecular weight of Fe<sub>3</sub>O<sub>4</sub>,  $M_{\text{Fe}_3\text{O}_4} = 231.53 \text{ g/mol}$ .

Number of moles of Fe<sub>3</sub>O<sub>4</sub>,  $n_{\text{Fe}_3\text{O}_4} = m/M = 4.32 \times 10^{-4} \text{ mol}$ .

Total number of moles of Fe (II, III),  $n_{\text{total}} = 3 \times n_{\text{Fe}_3\text{O}_4} = 1.30 \times 10^{-3} \text{ mol}$ .

So, the total number of moles of Fe (II, III) available in 100 mg of iron oxide powder is  $1.30 \times 10^{-3} \text{ mol}$ , BUT not all of this is exposed to the rolling oil for catalysis since the iron is present as 5 μm particles.

##### 5.3.2.1.2 Fraction of Fe (II, III) Available on the Surface of Each 5 μm Particle

Surface area of a 5  $\mu\text{m}$  sphere =  $4\pi r^2 = 78.54 \mu\text{m}^2$ .

Volume of a 5  $\mu\text{m}$  sphere =  $4/3\pi r^3 = 65.45 \mu\text{m}^3$ .

Surface-to-volume ratio =  $78.54 \mu\text{m}^2 / 65.45 \mu\text{m}^3 = 1.2$ .

So, the number of moles of iron exposed to the rolling oil for catalysis,  $n_{\text{catalysis}}$ , is given by  $n_{\text{catalysis}} \text{Fe} = 1.2 \times 1.30 \times 10^{-3} \text{ mol} = 1.56 \times 10^{-3} \text{ mol}$ .

Therefore, there are  $1.6 \times 10^{-3}$  moles of iron available for reaction with each 100 mg of rolling oil in the 50 % w/w iron oxide powder tests.

### 5.3.2.2 6 mm Diameter Steel Puck

The oil/steel samples analysed by TGA in section 5.1 were prepared by spreading  $\sim 1$  mg of rolling oil onto the surface of a 6 mm diameter cold rolled steel puck.

The following assumptions are used in these calculations:

- exactly 1 mg of rolling oil is used;
- the steel puck is exactly 6 mm in diameter;
- the surface of the steel is perfectly flat (surface roughness is not accounted for);
- the iron present in the steel is in the 0 oxidation state (metallic Fe), and
- the cold rolled steel is completely comprised on ferrite.<sup>57</sup>

#### 5.3.2.2.1 Steel Puck Surface Area, $A_{\text{puck}}$

$A_{\text{puck}} = \pi r^2 = 88.83 \text{ mm}^2 = 8.88 \times 10^{19} \text{ pm}^2$ .

#### 5.3.2.2.2 Number of Ferrite Unit Cells on the Puck Surface

Ferrite has a body-centred cubic structure (bcc).<sup>57</sup>

The atomic radius,  $a_0$  of  $\text{Fe}^0$  is 125 pm.<sup>58</sup>

In order to determine the number of ferrite unit cells on the surface of the steel puck, the surface area of each cell,  $A_{\text{cell}}$ , is calculated as follows.

The lattice parameter,  $a$ , of a ferrite unit cell is given by  $2a^2 = (4 \times a_0)^2$ ;  $a = 356 \text{ pm}$ .

Surface area of a ferrite unit cell =  $356 \text{ pm} \times 356 \text{ pm} = 127008 \text{ pm}^2$ .

Therefore, the number of steel unit cells on the surface of each steel puck (# cells) is determined by  $\# \text{ cells} = 8.88 \times 10^{19} \text{ pm}^2 / 127008 \text{ pm}^2 = 7 \times 10^{14}$  unit cells.

There are two Fe atoms per bcc unit cell of steel, so that the number of atoms of Fe is  $(7 \times 10^{14}) \times 2 = 1.4 \times 10^{15}$  atoms.

The number of moles of Fe,  $n_{\text{Fe}}$ , on the surface area of the puck is  $n_{\text{Fe}} = 1.4 \times 10^{15} / N_{\text{A}} = 2.3 \times 10^{-9}$  mol.

Therefore, there are  $2.3 \times 10^{-7}$  moles of iron available for reaction with each 100 mg of rolling oil in the 6 mm diameter steel puck tests.

### 5.3.2.3 Industrial Cold Rolling Process

In the industrial cold rolling process, there is  $\sim 600$  mg of oil per  $\text{m}^2$  of steel.<sup>59</sup>

The following assumptions are used in these calculations:

- exactly 600 mg of rolling oil is present per  $\text{m}^2$  of steel;
- the surface of the steel is perfectly flat (surface roughness is not accounted for);
- the iron present in the steel is in the 0 oxidation state (metallic Fe)
- no iron fines are present on the surface, and
- the steel is completely comprised of ferrite.<sup>57</sup>

#### 5.3.2.3.1 Number of Ferrite Unit Cells per $\text{m}^2$ of Cold Rolled Steel Surface

Steel surface area =  $1 \times 10^{24} \text{ pm}^2$ .

Ferrite unit cell surface area =  $127008 \text{ pm}^2$ .

$\# \text{ cells} = 1 \times 10^{24} \text{ pm}^2 / 127008 \text{ pm}^2 = 7.9 \times 10^{18}$  unit cells.

There are two Fe atoms per bcc unit cell of steel, so that the number of atoms of Fe is  $(7.9 \times 10^{18}) \times 2 = 1.6 \times 10^{19}$  atoms.

Number of moles of Fe per surface area =  $1.6 \times 10^{19} / N_{\text{A}} = 2.6 \times 10^{-5}$  mol.

Therefore, there are at least  $4.4 \times 10^{-6}$  moles of iron available for reaction with each 100 mg of rolling oil on the cold rolled steel surface.

### 5.3.3 Summary

The iron:oil ratios present in a 50 % w/w oil/iron oxide powder mixture, when 1 mg of rolling oil is placed onto the surface of a 6 mm diameter steel puck and during industrial cold rolling have been theoretically calculated and are summarised in table 5.7.

**Table 5.7 Summary of iron:oil ratios.**

Sample Configuration	Iron per 100 mg of Rolling Oil (mol)
50 % w/w oil/iron oxide mixture	$1.6 \times 10^{-3}$
1 mg oil on a 6 mm diameter steel puck	$2.3 \times 10^{-7}$
Industrial cold rolling process	$4.4 \times 10^{-6}$

### 5.4 References

1. Hasenhuettl, G. L., Fats and Fatty Oils. In *Kirk-Othmer Encyclopedia of Chemical Technology*, Kroschwitz, J. I., 'Ed.'; John Wiley & Sons: New York, 2005; pp 801.
2. Han, S., Chang, C. D., Fuels, Synthetic, Liquid Fuels. In *Kirk-Othmer Encyclopedia of Chemical Technology*, Kroschwitz, J. I., 'Ed.'; John Wiley & Sons: New York, 2000; pp 1.
3. Zhang, Y., Pei, P., Perez, J. M., Hsu, S. M., *Lubr. Eng.* **1992**, *48*, 189.
4. Zhang, Y., Perez, J. M., Pei, P., Hsu, S. M., *Lubr. Eng.* **1992**, *48*, 221.
5. Adhvaryu, A., Erhan, S. Z., Sahoo, S. K., Singh, I. D., *Fuel* **2002**, *81*, 785.
6. Adamczewska, J. Z., Love, C., *J. Therm. Anal. Cal.* **2005**, *80*, 753.
7. Sharma, B. K., Stipanovic, A. J., *Thermochim. Acta* **2003**, *402*, 1.
8. Du, D., Kim, S. -S., Moon, W. -S., Jin, S. -B., Kwon, W. -S., *Thermochim. Acta* **2003**, *407*, 17.
9. Zeman, A., Stuwe, R., Koch, K., *Thermochim. Acta* **1984**, *80*, 1.
10. Kauffman, R. E., Rhine, W. E., *Lubr. Eng.* **1988**, *44*, 154.
11. Santos, J. C. O., Santos, I. M. G., Souza, A. G., Sobrinho, E. V., Fernandes Jr., V. J., Silva, A. J. N., *Fuel* **2004**, *83*, 2393.
12. Willem, J.-F., Claessens, S., Cornil, H., Fiorucci, M., Hennion, A., Xhoffer, C. In

*Solidification mechanisms of aluzinc coatings - effect on spangle size*, Galvatech '01 - Proc. 5th Int. Conf. on Zinc and Zinc Alloy Coated Steel Sheet, Brussels, Belgium; 2001, pp 401.

13. Tang, N.-Y., Goodwin, F. E. In *A study of defects in galvanized coatings*, Galvatech '01 - Proc. 5th Int. Conf. on Zinc and Zinc Alloy Coated Steel Sheet, Brussels, Belgium; 2001, pp 49.

14. Chen, F., Patil, R. In *An in-depth analysis of various subtle coating defects of the 2000's*, Galvatech '04 - Proc. 6th Int. Conf. on Zinc and Zinc Alloy Coated Steel Sheet, Chicago, USA; 2004, pp 1055.

15. Puente, J. M., Alonso, F. J., Andres, L., Prado, M. In *Influence of an adequate surface conditioning on the final characteristics of GI for exposed panels use on automotive sector*, Galvatech '04 - Proc. 6th Int. Conf. on Zinc and Zinc Alloy Coated Steel Sheet, Chicago, USA; 2004, pp 457.

16. Lafargue, P. E., Chaoui, N., Millon, E., Muller, J. F., Derule, H., Popandec, A., *Surf. Coat. Technol.* **1998**, 106, 268.

17. Hombek, R., Heenan, D. F., Januszkiewicz, K. R., Sulek, H. H., *Lubr. Eng.* **1989**, 45, 56.

18. Osten-Sacken, J., Pompe, R., Skold, R., *Thermochim. Acta* **1985**, 95, 431.

19. Treverton, J. A., Thomas, M. P., *Int. J. Adhes. Adhes.* **1989**, 9, 211.

20. Sech, J. M., Oleksiak, T. P., *Iron Steel Eng.* **1995**, 72, 33.

21. Suilen, F., Zuurbier, S. In *Fundamental aspects of gas-metal reactions during batch annealing in 100% hydrogen*, Proc. 38th Mechanical Working and Steel Processing Conference, Ohio, USA; 1997, pp 375.

22. Gines, M. L. J., Benitez, G. J., Perez, T., Bossi, E. In *Surface reactions during batch annealing process*, Proc. 55th Annual ABM Congress, Rio de Janeiro; 2000, pp 2239.

23. Abou El Naga, H. H., Salem, A. E. M., *Wear* **1984**, 96, 267.

24. Tamai, Y., Sumimoto, M., *Lubr. Eng.* **1975**, 31, 81.

25. Gamlin, C. D., Dutta, N. K., Choudhury, N. R., Kehoe, D., Matisons, J., *Thermochim. Acta* **2002**, 392-393, 357.

26. Blanco, A., Renshaw, W., *Thermogravimetric set-up for oil volatility tests*; BHP Steel: 1998; pp 1.
27. Blanco, A., Took, P., *The effects of slow coil cooling on the ageing and volatility of cold rolling lubricants - part 2*; BHP Steel: 1999; pp 1.
28. Blanco, A., Took, P., *The effects of slow coil cooling on the ageing and volatility of cold rolling lubricants*; BHP Steel: 1999; pp 1.
29. Sridhar, S. In *Application of confocal laser microscopy to steel research*, ICS 2005, Charlotte, North Carolina, USA; 2005, pp 797.
30. Phelan, D., Reid, M., Dippenaar, R., *Metall. Mater. Trans. A* **2006**, 37A, 985.
31. Flynn, J. H., Wall, L. A., *Polymer Lett.* **1966**, 4, 323.
32. Ozawa, T., *B. Chem. Soc. Jpn.* **1965**, 38, 1881.
33. Ozawa, T., *J. Therm. Anal.* **1970**, 2, 301.
34. Blaine, R., *Am. Lab.* **1998**, 30, 21.
35. Blaine, R. L., Hahn, B. K., *J. Therm. Anal. Cal.* **1998**, 54, 695.
36. Blaine, R. L. Method and apparatus of modulated-temperature thermogravimetry. US 6113261, 2000.
37. Gracia-Fernandez, C. A., Gomez-Barriero, S., Ruiz-Salvador, S., Blaine, R., *Prog. Org. Coat.* **2005**, 54, 332.
38. Dweck, J., Sampaio, C. M. S., *J. Therm. Anal. Cal.* **2004**, 75, 385.
39. Oyman, Z. O., Ming, W., van der Linde, R., *Prog. Org. Coat.* **2005**, 54, 198.
40. Liu, C., Yu, J., Sun, X., Zhang, J., He, J., *Polym. Degrad. Stab.* **2003**, 81, 197.
41. Santos, J. C. O., Santos, I. M. G., Conceicao, M. M., Porto, S. L., Trindade, M. F. S., Souza, A. G., Prasad, S., Fernandes, V. J., Araujo, A. S., *J. Therm. Anal. Cal.* **2004**, 75, 419.
42. Kasprzycka-Guttman, T., Odzeniak, D., *J. Therm. Anal.* **1993**, 39, 217.
43. Blaine, R. L.
44. Mamleev, V., Bourbigot, S., *Chem. Eng. Sci.* **2005**, 60, 747.
45. Svedung, D. H., *Scand. J. Metall.* **1980**, 9, 183.
46. Chopra, A., Sastry, M. I. S., Kapur, G. S., Sarpal, A. S., Jain, S. K., Srivastava, S. P.,

- Bhatnagar, A. K., *Lubr. Eng.* **1995**, 52, 279.
47. Browne, K. M. Available energy: unified concepts for classical and irreversible thermodynamics. Deakin University, Geelong, 2001.
48. Keyser, A. G., Kunkel, K. F., Snedaker, L. A., *Iron Steel Eng.* **1998**, 75, 43.
49. Tanikawa, K., Fujioka, Y., *Lubr. Eng.* **1984**, 40, 715.
50. Sathivel, S., Prinyawiwatkul, W., Negulescu, I., King, J., Basnayake, B., *J. Am. Oil Chem. Soc.* **2003**, 80, 1131.
51. Frankel, E. N., *Prog. Lipid Res.* **1985**, 23, 197.
52. Adhvaryu, A., Erhan, S. Z., Liu, Z. S., Perez, J. M., *Thermochim. Acta* **2000**, 364, 87.
53. Cheenkachorn, K., Lloyd, W. A., Perez, J. M. In *The use of pressurized differential scanning calorimetry (PDSC) to evaluate effectiveness of additives in vegetable oil lubricants*, ASME ICES03, Spring Technical Conference, Internal Combustion Engine Division, Saltzburg; May 11-15, 2003, pp 197.
54. Rice, F. O., Herzfeld, K. F., *J. Am. Chem. Soc.* **1934**, 56, 284.
55. Dionne, S., Voyzelle, B., Li, J., Essadiqi, E., Baril, E., McDermid, J. R., Goodwin, F. In *Effect of reheating parameters of galvanizing behaviour and properties of high strength hot rolled steels*, Galvatech '04 - Proc. 6th Int. Conf. on Zinc and Zinc Alloy Coated Steel Sheet, Chicago, USA; 2004, pp 751.
56. Ninan, K. N., Krishnan, K., Rao, K. V. C. In *A thermogravimetric study of the catalytic decomposition of non-edible vegetable oils*, Thermal Analysis - Proc. 7th Int. Conf. on Thermal Analysis, 1982, pp 1197.
57. Askeland, D. R., *The Science and Engineering of Materials*. 3rd ed.; Stanley Thornes: Cheltenham, UK, 1998.
58. Huheey, J. E., Keiter, E. A., Keiter, R. L., *Inorganic Chemistry: Principles of Structure and Reactivity*. 4th ed.; HarperCollins College Publishers: New York, USA, 1993.
59. Gibson, A., Pers. Comm. In 2003.